ILASS-Americas 22nd Annual Conference on Liquid Atomization and Spray Systems, Cincinnati, OH, May 2010

High-Speed Shadowgraphy Investigations of Superheated Liquid Jet Atomisation

H. Kamoun[*], G. Lamanna, B. Weigand
Institute of Aerospace Thermodynamics
Universität Stuttgart, 70569 Stuttgart Germany

J. Steelant
ESTEC-ESA, 2200 AG Noordwijk, The Netherlands

Abstract

This paper investigates the characteristics and morphology of a flash-atomising jet by means of high-speed shadowgraphy. The primary goal is to derive a unified model for predicting the lateral spreading of the jet. As a first step, a new test bench is designed for performing flash atomisation experiments at well-defined and reproducible test conditions. The experiments are carried out with ethanol, acetone and iso-octane, injected from a small nozzle ($D = 150\mu$m, $L/D = 6$) into a vacuum chamber. The chamber is equipped with a fast-response, temperature controlled injector. The experiments are performed at ambient temperature and chamber pressure p_∞, varying between 0.02 and 0.4 bar. The injection pressure is fixed to 10 bar and the injection temperature T_{inj} varies between 30 and 147 °C. The high-speed images enable the visual inspection of the flashing jet structure and geometry. For low superheat conditions, mechanical breakup prevails. By increasing the superheat of the liquid jet, transition towards the fully flashing disintegration regime is observed. In the flash-atomisation regime, the spreading angle is an increasing function of superheat, while the average droplet diameter decreases steadily. For the analysis of the high-speed images, it is postulated that bubble nucleation is the predominant mechanism controlling the shattering of the jet and its lateral spreading in the near-nozzle region. By expressing the jet angle as function of the two driving forces for bubble nucleation, a single analytical function is derived to predict the spray contour. The correlation is valid over a wide range of superheating, back pressures, injection temperatures and different fluids. This indirectly confirms that both the physics of the problem is well captured by the proposed correlation and that the initial assumption on the predominance of the nucleation process is well-founded.

---

[*] Corresponding Author: itlhka@itlr.uni-stuttgart.de

Introduction

Flash-atomisation occurs when a liquid is injected into a combustion chamber where the ambient pressure is lower than the saturation pressure of the fuel. The inception of flashing strongly depends on the level of superheat and on the transient heat conduction process within the depressurised liquid jet. If the energy excess cannot be conducted at sufficiently high rate towards its surface, phase transition will occur within the liquid jet through nucleation and bubble growth. Liquid jet disintegration (i.e. the actual atomisation) is then a consequence of bubble bursting. Although flash-boiling is considered to be detrimental in many technical applications (e.g. the accidental release of flammable and toxic pressure-liquefied gases in nuclear and chemical industry), it can have some potential benefits in propulsion systems as it is known to produce a fine spray with enhanced atomisation, increase the effective spray angle, and decrease spray penetration. These significant changes in the spray characteristics have therefore an important impact on the fuel oxidant mixing and hence on combustion efficiency.

From a heuristic point of view, the process of flash-atomisation and vaporisation is clearly described as the subsequent progression of homogeneous (or heterogeneous) nucleation, bubble growth [1], breakup through bubble disruption, and (superheated) droplet evaporation. Due to its relevance for automotive and industrial applications, considerable progress has been made in the modelling and experimental investigation of a flash-atomising liquid spray at atmospheric conditions. Oza [2] investigated the mechanisms responsible for flash boiling and identified two regimes:

- an internal mode, characterised by formation of two-phase flow inside the nozzle
- an external mode, where phase change occurs outside the nozzle.

The specific sequence for external and internal flashing is shown in Fig. 1. Park and Lee [3] confirmed these findings and suggested a length-to-diameter ratio (L/D) of seven for the transition between the two modes. They measured drop sizes and found the Sauter mean diameter (SMD) to be a decreasing function of superheating. A detailed review on the subject can be found in [4, 5]. The critical superheat of flashing water/ethanol jets was derived experimentally by Kitamura et al. [6], who proposed an empirical correlation for predicting the onset of flash atomisation. More recently, Cleary et al. [7] extended this model by including the transition from mechanical breakup to full flashing. The experimental data are reduced via non-dimensionalisation in terms of the Weber and Jakob number, representing the fluid mechanics and thermodynamics of the system, respectively. The fluid utilised throughout is water, flashing at ambient pressure. Verification of model performance is therefore required for other fluids and back pressures.

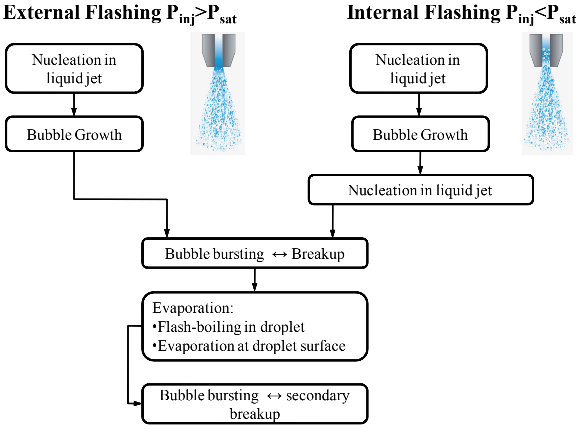

Figure 1. Schematic of flash-atomization and vaporization

The experimental investigation and modelling of highly superheated jets (e.g. as encountered at very low back pressures) have received, instead, less attention, due to the difficulty of maintaining the ambient pressure constant at near vacuum conditions. Kurschat et al. [8] were among the first to investigate the evaporation of highly superheated liquid jets. They modelled the evaporation as a sonic deflagration followed by an axisymmetric supersonic expansion of a two-phase flow. Their analysis has been further extended by Vieira and Moreira [9, 10]. They showed that, at extreme conditions (i.e. very low back pressures), the rapid and intense phase-change process is limited by a maximum mass flow rate condition. The latter is known as the Chapman-Jouguet point in analogy to a deflagration wave in a combusting gas. These findings are particularly relevant for space propulsion systems, operating at near-vacuum conditions, and indicate a limit for the theoretical admissible vaporisation rate for a flash-disintegrating liquid jet.

In general, the quality of a flashing-spray is evaluated in terms of empirical correlations for droplet sizes, velocity distributions, jet spreading angle, and penetration lengths: Wiltox et al. [11, 5], Cleary et al. [7], Yildiz et al. [12, 13] for atmospheric conditions; Lecourt et al. [14] for near vacuum conditions.

The proposed correlations have the merit to lead to an engineering model for the rapid and efficient characterisation of a flash-atomising liquid jet. Unfortunately their range of applicability is rather limited, being restricted to the particular fluids (namely water and ethanol) and operating conditions tested. In a recent paper, Cleary et al. [7] tried to extrapolate their empirical model to other fluids through similarity scaling. Despite the noteworthy attempt, there is still considerable research and development required to appraise, verify and corroborate the proposed extrapolation technique.

The present study aims at providing a comprehensive and accurate database on flash atomisation for model validation purposes. The database should include data on spray morphology as well as on droplet size, velocity and temperature distributions. As a first step, the transition criteria for the onset of flashing, developed by Cleary et al. [7] for water/ethanol jets at atmospheric conditions, is verified for other fluids and highly superheated jets (i.e. very low back pressure). Second, a generalised model is proposed to predict the spray contour, that is the spreading angle as function of the axial distance. This extended model should be applicable to different fluids, back pressures and superheat levels. The rationale for the model development is outlined in details in the result section. The paper is organised as follows. The section "Flashing" reviews briefly the most relevant non-dimensional parameters governing the flash atomisation and bubble nucleation processes. The test facility and the post-processing algorithms are described in the section "Experimental Setup". Finally, the section "Results and Discussion" discusses the modelling strategy, the experimental results and verifies the accuracy of the proposed model.

Flashing

As mentioned in the introduction section, the process of nucleate boiling concerns mostly superheated fluids. The superheat level can be described through two parameters, indicated in Fig. 2. They are related to either the pressure difference $\Delta p = p_{sat}\left(T_{inj}\right) - p_\infty$ or the temperature difference between a superheated liquid and the saturated bulk vapour.

The first parameter (ΔT - alias the degree of superheat) is defined as the difference between the fuel injection temperature and the saturation temperature at the assigned back pressure:

$$\Delta T = T_{inj} - T_{sat}\left(p_\infty\right) \tag{1}$$

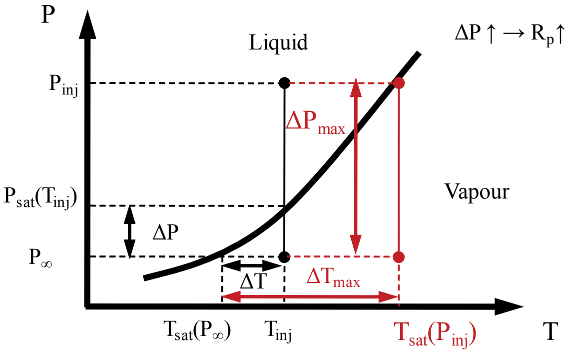

Figure 2. Flashing parameters

In a liquid system, it is a measure for the temperature excess with respect to the liquid boiling (i.e. equilibrium) temperature at the prescribed ambient pressure.

The second parameter R_p is defined as the ratio between the saturation pressure at the fuel injection temperature and the prescribed back pressure:

$$R_p = \frac{p_{sat}\left(T_{inj}\right)}{p_\infty} \tag{2}$$

For an isothermal process (as nucleate boiling), the Gibbs-Duhem relation reduces to

$$\Delta\mu = -sdT + vdp = vdp \tag{3}$$

As can be seen, the pressure difference between a superheated liquid and the saturated bulk vapour is directly related to the difference in chemical potential, which represents the "generalised driving force" for the phase transition process. It is therefore reasonable to expect that the parameter R_p plays a dominant role for the bubble nucleation process. In the realm of Classical Nucleation Theory (CNT), the nucleation rate J, i.e. the number of stable vapour nuclei generated per volume and time, decreases exponentially with the Gibbs free energy ΔG_n [15]:

$$J \propto \sqrt{\frac{\sigma}{m}} exp\left(\frac{-\Delta G_n}{k_b T_{inj}}\right) \tag{4}$$

where ΔG_n is defined as:

$$\Delta G_n = \frac{16\pi\sigma^3}{3\left(1-\frac{1}{R_p}\right)^2 p_{sat}^2} \tag{5}$$

Following Girshick and Chiu [16], let us introduce a dimensionless surface tension Θ:

$$\Theta = \frac{a_0\sigma}{k_b T_{inj}} \tag{6}$$

where k_b represents the Bolzman constant, a_0 is the molecular surface area defined as $a_0 = (36\pi)^{1/3}(v_l)^{2/3}$ and v_l is the liquid molecular volume. The parameter Θ measures the relative importance between surface energy (i.e. the energy required for the creation of a new interface) and thermal energy. Combining the Eqs. (4), (5) and (6), the nucleation rate can be expressed as:

$$J \propto \sqrt{\frac{\sigma}{m}} exp\left[-\frac{4}{27}\Theta^3\left(\frac{\rho_l}{\rho_v}\right)^2 \frac{1}{\left(1-\frac{1}{R_p}\right)^2}\right] \quad (7)$$

Under the assumption of a nucleation-controlled shattering of a superheated jet (at least limitedly to the near-nozzle region), the two non-dimensional parameters R_p and Θ appear as the most natural choice for efficiently reducing the spray angle data into a single and meaningful model. The validity of this assumption is verified in the result section.

Experimental Set-up

Test facility

The test bench is designed for performing flash atomisation and vaporisation experiments at low pressure and medium vacuum conditions. In order to attain a pressure ratio value as high as R_p= 1000, the fuel can be heated up to 155 °C and the ambient pressure set at 0.005 bar. The operating conditions for the facility have been summarised in Table 1.

Parameter	Range
Injection pressure p_{inj}	$10 - 25$ bar
Injection temperature T_{inj}	$35 - 155\,°$C
Back pressure p_∞	$0.005 - 0.4$ bar
Pressure ratio R_p	$0.3 - 1000$

Table 1. Overview of test conditions that can be attained in the ITLR test bench

A schematic layout of the facility is shown in Fig. 3.

The test facility is composed of:

- a pressurising and venting system
- a liquid tank
- a modified automotive injector
- a windowed injection chamber connected to a large vacuum tank
- a vacuum pump

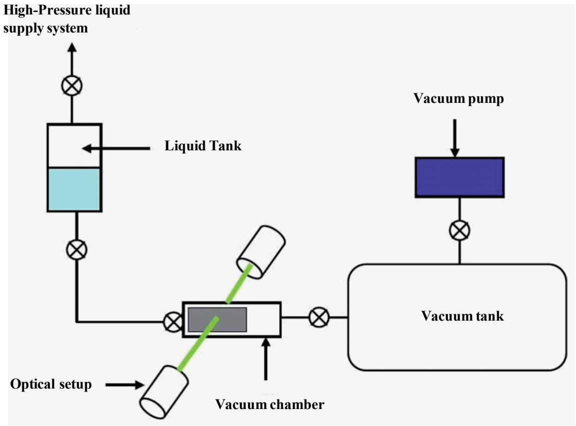

Figure 3. Schematic layout of the test facility

For the correct operation of the injector, a constant pressure has to be applied at the nozzle inlet. The liquid fuel is, in fact, forced through a capillary tube and a nozzle into the vacuum chamber. A gas bottle (typically nitrogen) is connected to the liquid reservoir and provides the driving force for pushing the liquid column through the nozzle. The latter has a diameter D of 150 μm and an exit orifice aspect ratio $L/D = 6$. With this setup, the injection pressure p_{inj} can be varied between 1 and 80 bar and maintained constant during an experimental run. The vacuum chamber can be either connected directly to a vacuum pump or to a voluminous tank, if a longer test-time is needed. To monitor the back pressure (p_∞), a vacuum transducers (MKS- Baratron 390) is connected to the vacuum chamber. A schematic view of the vacuum chamber is shown in Fig. 4.

The cylindrical test section is 300 mm long and has an internal diameter of 250 mm. Four circular windows ($\phi = 150$ mm) are installed at 90 deg apart from each other to allow visualisation of the spray and optical diagnostics. To monitor the temperature along the vacuum chamber, three thermocouples are flush-mounted along its walls. On the top flange, a heated fuel injector is mounted, as shown in Fig. 5. The injector chosen is a standard automotive fuel injector, which has been modified for low-pressure applications. It has got a characteristic response time of roughly 0.4 ms and is capable of establishing steady-state conditions within about 1 ms. Short transient times can be achieved by storing pressurised fuel inside the injector, thus strongly reducing the nozzle flow start-up time. Thereby fuel pressurisation and injection are decoupled, which facilitates the regulation of the fuel temperature as well. This implies that the fuel can be directly heated

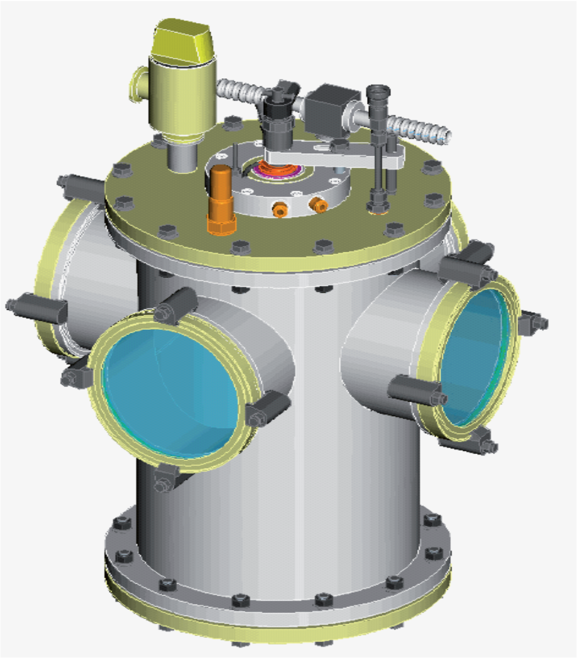

Figure 4. Vacuum chamber

within the injector itself so that the target fuel temperature is immediately obtained at the beginning of the injection event. With the present setup, injection times of 10 ms could be achieved with no appreciable change in back pressure. Table 2 offers a comparison between the stability of our test conditions compared to other facilities employed for similar studies.

	Lecourt [14]	Simoes-Moreira [9]	ITLR
Injection time	10 s	4 s	20 ms
Rate of pressure increase	118 Pa/s	45 Pa/s	<13 Pa/s
pressure increase during test time	1180 Pa	180 Pa	<0.26 Pa

Table 2. Constancy of pressure during test time: comparison among different facilities

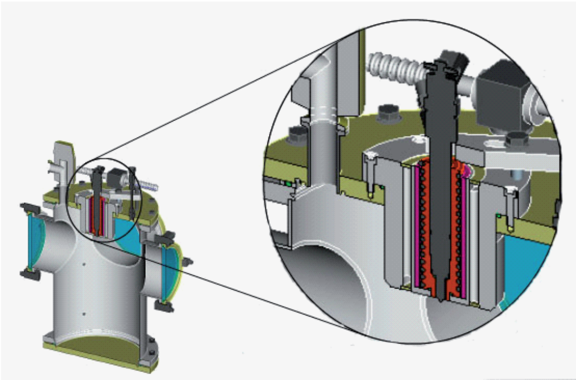

Figure 5. Details of the heating system

Optical setup

The optical layout of the shadowgraph setup is shown in Fig. 6. In order to minimise motion blur, the exposure time of the camera is set to 1μs. As the light source, a high luminosity LED is used to back illuminate the spray to compensate for the short acquisition time. The light is collected by a parabolic mirror and focused on the camera's chip (Photron Fastcam SA1) by an objective lens. The high-speed camera has a maximum resolution of 1024x1024 pixel at 5400 fps. For the present investigations, the camera resolution has been adapted to the region of interest, resulting in a higher frame rate. The resolution and magnification settings applied in the test runs are summarised in Table 3.

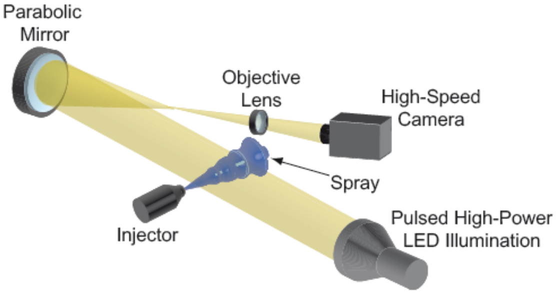

Figure 6. Optical setup [17]

Resolution	Frame rate	Magnification
256 x 784	22500 fps	1:4
512 x 440	30000 fps	1:1

Table 3. High-speed camera settings

Post-Processing

This section describes the post-processing algorithm, used to extract the spray geometrical data from the high-speed shadowgraphy images. The code is based on Matlab and was developed by Stotz et al. [17]. For accurate results, the image processing algorithm must reduce the background noise and enhance the image contrast without altering the spray contour. As a first step, illumination inhomogeneities due to temporal fluctuations as well as spatial non-uniformities of the light distribution are corrected by normalising each image to a reference image. In this way, the background intensity of all images from an experimental series is homogeneously distributed and set at a constant value. Then a median filter is applied to the normalised images to reduce the background noise, without affecting the shape of the spray. Afterwards, the spray images are thresholded to separate the spray from the background. Figure 7 illustrates schematically the three different phases of the image processing scheme.

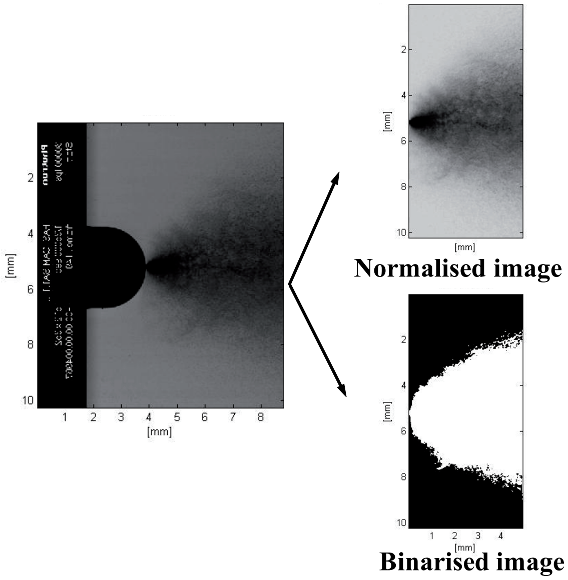

Figure 7. Image processing scheme

Once the spray contour has been defined, its upper and lower branch $y_i(x)$ are subsequently used to calculate the upper and lower half of the local spreading angles $\theta_i(x)$ according to

$$tan\left[\theta_i(x)\right] = \frac{y_i(x) - y_i(1)}{\Delta x}, \quad i = upper, lower \quad (8)$$

The total spray angle, shown in Fig. 8, is then calculated at different axial positions ($x/D = 2$, $x/D = 5$, $x/D = 10$, $x/D = 20$, $x/D = 60$) as:

$$\theta(x) = \theta_{upper}(x) - \theta_{lower}(x) \quad (9)$$

By applying Eq. (9) to all acquired images, temporally and spatially resolved information on the lateral spreading of the jet is gained.

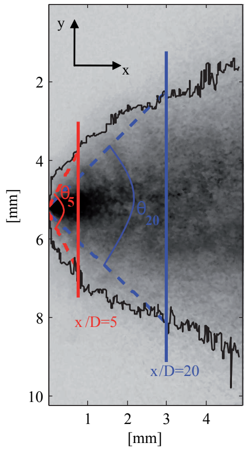

Figure 8. Definition of the local jet spreading angle

Results and Discussion

This section summarises and reviews critically the main findings from the high-speed shadowgraphy campaign on superheated jet atomisation. The section is divided in four chapters: Selection of test Matrix, Transition Condition, Spreading Angle and Model Verification.

Selection of Test Matrix

As the test fluids, acetone, ethanol and isooctane are selected. The rationale for this choice is twofold: 1) to facilitate comparison with literature data; 2) to include in the test matrix highly superheated conditions, as encountered in spacecraft operations. The test conditions are summarised in the Table 4 - 6.

Parameter	**Range**
Injection pressure p_{inj} [bar]	10
Injection temperature T_{inj} [°C]	35 - 116
Back pressure p_{∞} [bar]	0.02 - 0.4
Pressure ratio R_p[-]	0.3 - 196
Superheating ΔT [K]	-21 - 113

Table 4. Ethanol test matrix

Note that the injection temperature is selected in such a way that T_{inj} is always smaller than the equilibrium temperature corresponding to the injection pressure $[T_{inj} < T_{sat}\left(p_{inj}\right)]$. This represents a necessary requisite to avoid boiling inside the liquid reservoir.

Parameter	**Range**
Injection pressure p_{inj} [bar]	10
Injection temperature T_{inj} [°C]	30 - 100
Back pressure p_{∞} [bar]	0.02 - 0.4
Pressure ratio R_p[-]	0.9 - 186
Superheating ΔT [K]	-1.3 - 126

Table 5. Acetone test matrix

Parameter	**Range**
Injection pressure p_{inj} [bar]	10
Injection temperature T_{inj} [°C]	40 - 147
Back pressure p_{∞} [bar]	0.02 - 0.4
Pressure ratio R_p[-]	0.32 - 165
Superheating ΔT [K]	-31 - 145

Table 6. Isooctane test matrix

Transition Condition

Figure 9 shows the changes in the jet morphology with increasing degree of superheat. For subcooled liquid jets ($R_p < 1$ or $\Delta T < 0$), mechanical breakup controls the disintegration process. In the present experiments, jet breakup occurs in the Rayleigh regime (Fig. 9 - top row left, $R_p = 0.949$) due to the low injection velocities.

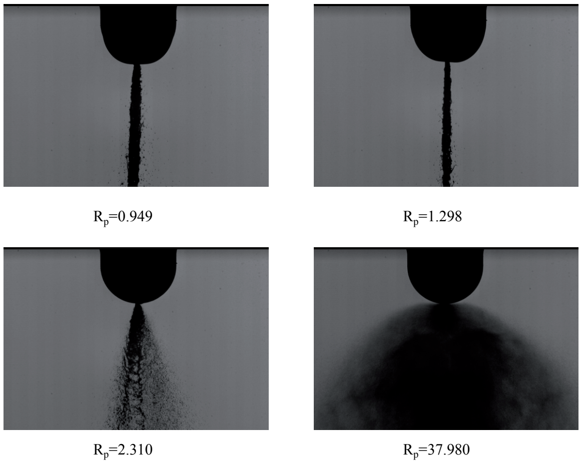

Figure 9. Spray geometry at different R_p. Fluid: ethanol. $p_{inj} = 10$ bar.

Mechanical breakup prevails also for low degrees of superheat (see Fig. 9 - top row right $R_p = 1.298$), since the onset of nucleation requires a high degree of superheating. By increasing the superheat level (alias R_p), a transition towards the fully flashing regime gradually occurs, as shown in Fig. 9 - bottom row left, $R_p = 2.310$. Within the transition region, the liquid jet still retains a liquid core of finite length. Flash boiling is confined to the periphery of the liquid core and results in a wide angled spray. By further increasing the parameter R_p, the full flashing regime sets in, as shown in Fig. 9 - bottom row right ($R_p = 37.98$). The jet disintegrates directly at the nozzle exit and assumes a bell shape configuration.

Cleary et al. [7] proposed an empirical correlation to predict the onset of flash atomisation. The intermediate region, separating the mechanical breakup from the fully flashing regime, is delimited by two points (A and C). Condition A identifies the onset of nucleate boiling, limitedly to the outermost part of the intact liquid core (e.g. Fig. 9, $R_p = 2.310$). Condition C represents the point beyond which the shape of the flashing jet does not change significantly with increasing superheat. The boundaries corresponding to condition A and C can be determined by means of the following empirical correlations:

$$\text{Start point A:} \quad Ja\Psi = 55 We_v^{-1/7} \tag{10}$$

$$\text{End point C:} \quad Ja\Psi = 150 We_v^{-1/7} \tag{11}$$

with:

$$\Psi = 1 - exp\left[-2300\left(\frac{\rho_v}{\rho_L}\right)\right] \tag{12}$$

where ρ_v is the vapour density evaluated at the chamber conditions, ρ_l is the liquid density evaluated at the orifice temperature, We_v is the vapour Weber number and Ja is the Jacob number. Following Kitamura [6], the vapour Weber number We_v and the Jacob number Ja are evaluated as

$$We_v = \frac{\rho_v u_0^2 D}{\sigma}; \quad Ja = \frac{c_{pl}\Delta T}{h_{fg}}\frac{\rho_l}{\rho_v} \tag{13}$$

The proposed model was verified for water and ethanol jets at atmospheric conditions. Figure 10 shows the classification of the present experiments following Cleary's transition model. The goal is to ascertain the accuracy of the model's predictions when applied to other fluids and near-vacuum conditions. As can be seen, highly superheated jets (i.e. high Ja numbers) disintegrate all in the fully flashing regime. To verify whether also the onset is correctly predicted, the transition criteria C was experimentally investigated for ethanol, acetone and iso-octane jets, flashing a near vacuum conditions. The results are plotted in Fig. 11. As can be noticed, all flash boiling data lie above the proposed correlation, regardless of the specific substance employed.

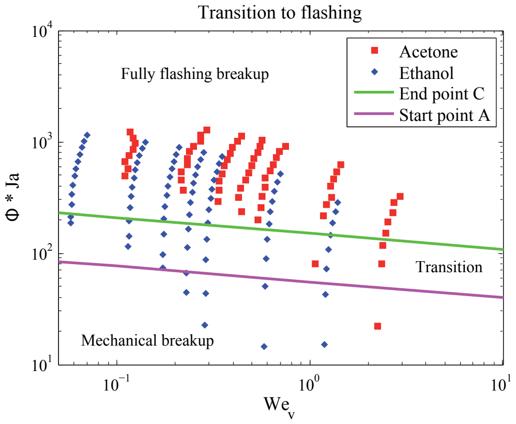

Figure 10. Transition criterion for flashing for ethanol and acetone

Small variations in fuel temperature (e.g. $\Delta T_{inj} \leq 1$) suffice in shifting the data point below the transition point C, thus confirming the validity of Cleary's model.

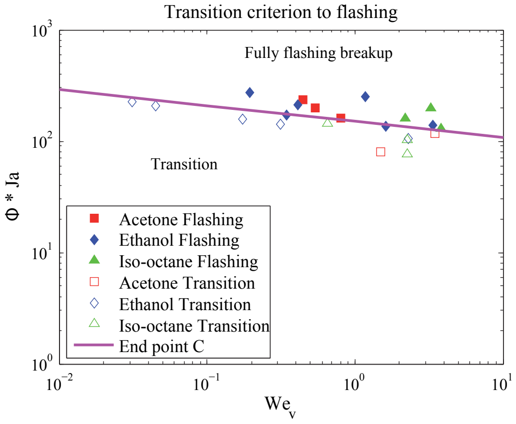

Figure 11. Transition criterion for flashing

Spreading Angle

The objective of this section is to derive a function for predicting the lateral spreading of a flash atomising jet as a function of axial distance (x/D) from the exit plane of the nozzle. The model should provide a realistic representation of the spray contour, thus constituting a reasonable initial conditions for spray simulations. Furthermore, the model should be valid over a wide range of back pressures, superheat levels and test fluids. To comply with the desired requirements, a precise rationale is followed.

First, the available literature data have been reviewed to obtain information on the physics of phenomena and to identify common denominators for describing the lateral spreading of a flashing jet under a variety of environmental conditions. Second, the controlling factors for flash atomisation have been grouped together in non-dimensional parameters and a correlation is proposed for the spray angle in externally flashing jets. The function is obtained correlating the data from ethanol, acetone and iso-octane superheated jets and is expressed in terms of dimensionless parameter only, in order to facilitate its generalisation to other substances. Third, the accuracy of the proposed model is verified by comparing the predicted spray contour with the experiments and by performing an uncertainty analysis. Finally, all available literature data on spray angle have been collected and compared with the predictions of the model to assess its applicability to other substances.

It appears that only few authors have dealt with the quantitative characterisation of the jet spreading angle ([3], [18, 19]). The principal obstacle in deriving a unified model is the considerable scatter in the available data. Each author evaluates the spray angle at completely different axial location, which makes the comparison and reduction of data rather impervious. The local value of the spray angle depends, in fact, upon two concomitant effects, namely flash boiling and gas entrainment, whose relative importance varies along the jet axial distance. A good review on the subject can be found in Park and Lee [3]. The authors investigated internal and external flashing modes in transparent nozzles. In both regimes, the same trend is obtained for the spreading angle as function of the superheat, but larger angles are observed in the internal flashing mode. The authors also reported that, in the downstream region of the spray ($x/D \geq 50$), the spray angle increases with the degree of superheat up to a certain value and then decreases. This phenomenon is due to air entrainment effects, which become predominant over the flashing effect further downstream from the exit nozzle plane.

Our experimental results confirm the trend observed by Park and Lee [3] and Nagai et al. [18]. Specifically, by evaluating the lateral jet spreading at different axial location, it is possible to distinguish between a near-nozzle ($x/D \leq 40$) and downstream region. In the near nozzle region, the lateral spreading of the liquid jet is strongly dominated by the bubble nucleation process. As a general rule of thumb, the higher the superheat level ΔT (alias $R_p \gg 1$), the higher the production of bubble nuclei, which leads to a more widespread process of bubble "bursting" and hence to a larger jet spreading angle. This trend is shown clearly in Fig. 12. For constant injection p_{inj} and back pressures p_∞, the spray angle increases initially with the injection temperature (i.e. degree of superheat). With reference to Fig. 10, this functional dependence is observed in the transition region and in the first stage of the "fully flashing" regime (i.e. beyond point C). Eventually, the spray angle reaches a maximum value (θ_{max}), corresponding to the condition ($T_{inj} \approx T_{sat}(p_{inj})$), which represents the maximum attainable superheating (alias R_p) at the prescribed injection pressure. This condition is depicted schematically in Fig. 2 (red line).

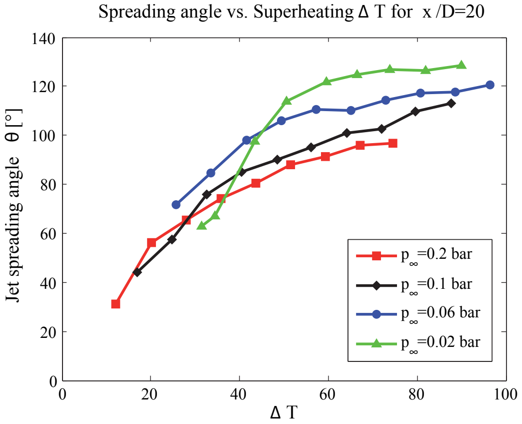

Figure 12. Spreading angle versus degree of superheating. Fluid: ethanol. p_{inj} = 10 bar. Location: $x/D = 20$

In the downstream region ($x/D > 40$), the spray angle increases with the injection temperature up to a certain value and then decreases, as shown in Fig. 13. The initial increase of the spray angle with the superheating is attributed to the related increase of nucleation rate. The subsequent drop in spray angle at a specific ΔT is attributed to entrainment effects. Due to enhanced nucleation and evaporation rates, the droplets reduce their size considerably and follow the gas flow. Thus by increasing the injection temperature, the entrainment effect becomes more dominant and the spray lateral spreading narrows down. This effect becomes increasingly relevant in the downstream region of the jet due to further flashing events and prolonged drop residence time in a superheated environment. Note that since the entrainment effect is strongly dependent upon flow conditions in the test chamber (which are not known a priori), the formulation of a predicting tool for the spray contour in this region is basically impossible. On the basis of these considerations, our modelling efforts will concentrate solely on the near-nozzle region and will be limited to externally fully flashing jets (i.e. beyond the transition condition C).

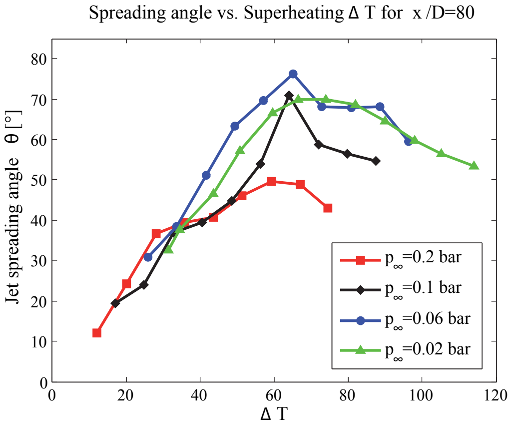

Figure 13. Spreading angle versus degree of superheating. Fluid: ethanol. p_{inj} = 10 bar. Location: $x/D = 80$

As a first step in the development of a model for the lateral spreading of a superheated jet, the literature data have been critically reviewed. As customarily done, most authors tried to correlate the normalised spreading angle θ_m with the dimensionless superheat ΔT^*. The normalised spreading angle θ_m is defined as the local spray angle divided by its maximum value $\theta_m = \theta/\theta_{max}$ (for a constant back pressure p_∞). The dimensionless superheat ΔT^* is defined as:

$$\Delta T^* = \frac{T_{inj} - T_{sat}(p_\infty)}{T_{sat}(p_{inj}) - T_{sat}(p_\infty)} \tag{14}$$

Following this approach, the local spray angle, evaluated at the axial location $x/D = 20$, is expressed as function of ΔT^* and shown in the Fig. 14. At all back pressures, the spray angle reaches its maximum θ_{max} in correspondence of $\Delta T^* = 1$ (max attainable superheat level). The latter represents the physical limit to flashing, since it implies boiling inside the liquid fuel reservoir [i.e. $T_{inj} = T_{sat}(p_{inj})$]. For an assigned saturation curve (i.e. liquid fuel), the specific value of θ_{max} depends upon the back pressure.

A major drawback in choosing ΔT^* as the independent variable is that the dependence of the spray angle on the back pressure is not correctly captured by the proposed correlation. This can be deduced from the fact that the different curves (for p_∞= const.) do not collide into a single one. This

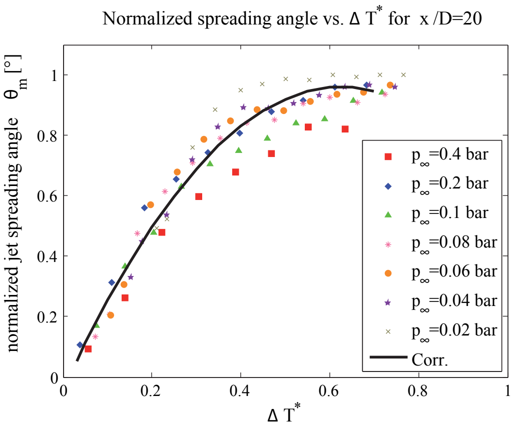

Figure 14. Normalised angle as function of ΔT^*. Fluid: ethanol. $p_{inj} = 10$ bar. Location: $x/D = 20$

is not surprising if bubble nucleation is the controlling process for the lateral spreading of the jet. As pointed out in the previous sections, the dimensionless superheat ΔT^* does not constitute, in fact, the relevant driving force for nucleation. Based on these considerations, the two non-dimensional parameters R_p and Θ have been chosen as the independent variables. With this choice of parameters, a single analytical function can be derived to predict the spray angle of a superheated ethanol jet as a function of $\log(R_p^2\Theta^3)$. The results are shown in Fig. 15. As can be seen, all curves for the different back pressure are basically merged into one single curve.

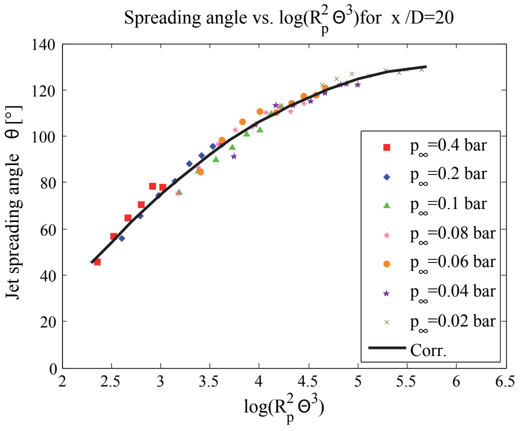

Figure 15. Spreading angle as function of $\log(R_p^2\Theta^3)$. Fluid: ethanol. $p_{inj} = 10$ bar. Location: $x/D = 20$

As a second step towards the development of a unified model, the applicability of this empirical correlation to other fluids, specifically iso-octane and acetone, has been attempted.

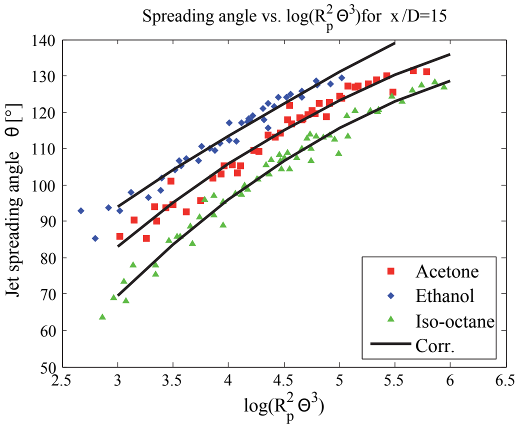

Figure 16. Spreading angle as function of $\log(R_p^2\Theta^3)$. $p_{inj} = 10$ bar. Location: $x/D = 15$

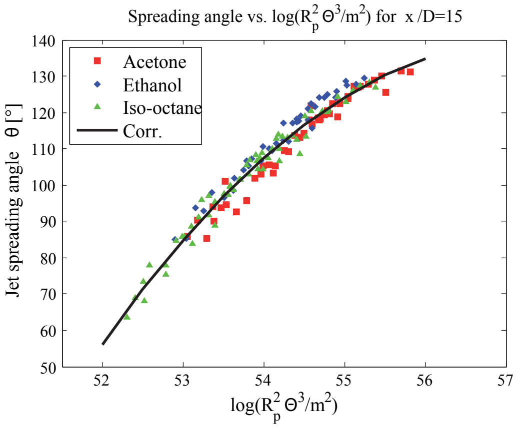

Figure 17. Generalised correlation for the local spray angle. Range of validity: $1 < R_p < 196$, 0.02 $< p_\infty < 1$ bar. $p_{inj} = 10$ bar. Location: $x/D = 15$

As can be seen in Fig. 16, the empirical functions for the different test fluids are basically parallel, but shifted with respect to each other by a constant quantity. It turns out that this constant is directly proportional (on a logarithmic scale) to the atomic mass m of each fuel. By shifting all curves by the fuel-dependent quantity $\log(m^2)$, all empirical correlations collapse to a single curve, as illustrated in Fig. 17. Note that the proposed function covers a wide range of test conditions both in terms of superheat levels and back pressures (as summarised in Table 4, 5, 6) and is not limited to a single test fluid.

This represents a noteworthy result if compared to the huge scatter in spray angle data, where for each test fluid and back pressures a new empirical correlation was presented.

As a third and final step towards the modelling of the lateral spreading of a flashing jet, the previous analysis has been extended to different axial positions, specifically ($x/D = 2, 5, 10, 15, 20$ and 40). For the nozzle used in this study, these locations correspond to a physical distance of 0.3, 0.75, 1.5, 2.25, 3.0 and 6.0 mm from the nozzle exit plane, respectively. The results are plotted in Fig.18. As can be seen, at all axial positions the data can be reduced to a single function. The data for the location $x/D = 20$ have not been included in the plot, as they basically overlap with the data acquired at $x/D = 15$ due to the barrel shape of the spray.

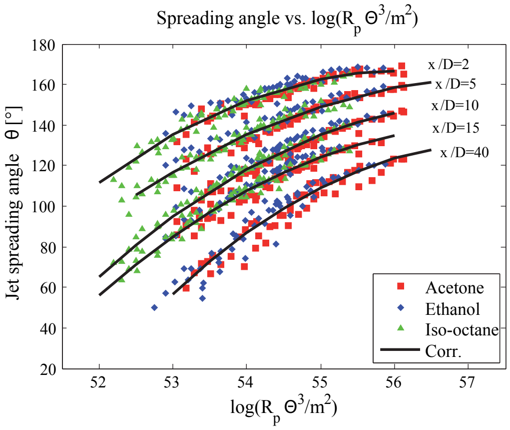

Figure 18. Generalised model for the local spray angle, evaluated at different axial position. Range of validity: $1 < R_p < 196$, $0.02 < p_\infty < 1$ bar. p_{inj} = 10 bar.

Denoting with ξ the non-dimensional group $\log\left(R_p^2\Theta^3/m^2\right)$, a single analytical function can be derived to predict the spray angle at each axial position. The most satisfactory results were obtained with a polynomial equation of second degree:

$$\theta = a\xi^2 + b\xi + c \tag{15}$$

The specific values for the coefficients a, b, c are reported in Table 7. The quality of the fit is measured by the coefficient of determination λ^2. This parameter relates the sum of squares of residuals to the sample variance. If $\lambda^2 \approx 1$, this implies that the most accurate fit has been obtained for the assigned data set, characterised by a specific sample variance.

x/D	a	b	c	λ^2
2	-3.234	363.07	-10021	0.931
5	-2.368	272.084	-7649	0.95
10	-3.208	366.61	-10324	0.962
15	-3.043	348.364	-9829	0.966
20	-2.851	332.92	-9559	0.933
40	-4.353	497.69	-14096	0.92

Table 7. Correlation parameters

Model Verification

This section reports the three basic verifications performed to assess the accuracy of the proposed model. This includes an uncertainty study, a comparison with literature data and the reconstruction of an experimental spray contour based on the predictions from the spray angle model.

The uncertainty in the experimental determination of the local spray angle is mostly due to the limited spatial resolution of the camera chip and to non-uniformities in the light distribution. They are responsible for the erroneous positioning of the spray contour during post-processing, and hence affect directly the reliability of the spray angle predictions. Since the spray angle is expressed as a function of the spray contour $\theta(x) = f\,[y(x)]$, its standard deviation y_{std} has been calculated at each axial position x, assuming as sample a population of 30 images. The random error is then determined as :

$$\Delta y_r = \frac{2y_{std}}{\sqrt{30}} \tag{16}$$

The systematic error depends upon the pixel size and is related to the impossibility to capture displacements of the jet contour within one pixel. Therefore the systematic error is fixed to $\Delta y_s = 20\,\mu$m (i.e. 1 pixel). By applying the Gaussian error propagation law to the global error ($\Delta y = \Delta y_r + \Delta y_s$), the corresponding inaccuracy in the determination of the spray angle can be determined. As an example, the latter is plotted as error bars in Fig. 19 for the axial position $x/D = 10$. Note that the largest error amounts to 3% and is observed mostly in highly superheated jets, thus providing good confidence in the reliability of the model predictions.

Concerning the capability of the model in predicting accurately the spray contour, Equation 15 is employed to reconstruct the lateral spreading of a flashing jet, for prescribed injection and test chamber conditions. The predicted contour is then compared with the experimentally determined one, as

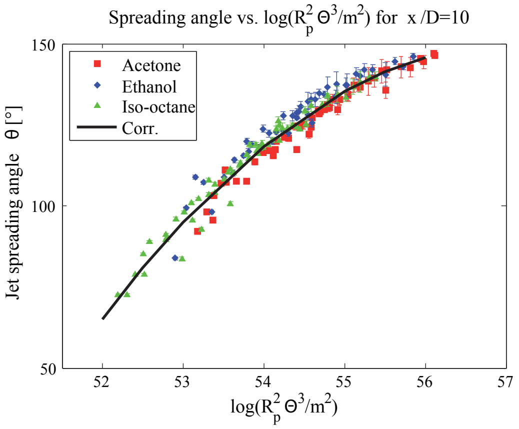

Figure 19. Generalised correlation for the local spray angle, with corresponding error bars. $p_{inj} = 10$ bar. Location: $x/D = 10$

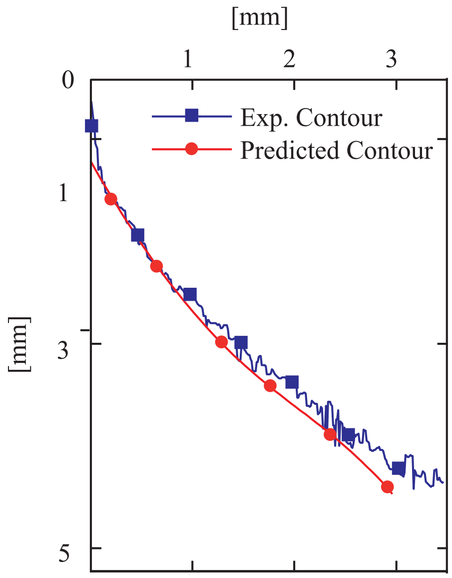

Figure 20. Comparison between experimental and reconstructed jet contour. Test conditions: $T_{inj} = 77°\text{C}$, $p_{inj} = 10$ bar, $p_\infty = 0.1$ bar. Fluid: acetone.

shown in Fig. 20. As can be seen, the predicted contour match the experimental data quite well. Note that the "thoretical" spray contour points have been connected to each other through a spline.

For the purpose of testing the applicability of the proposed model to other fluids, nozzles and test conditions, all relevant literature data on the local spray angle of a flashing jet have been collected and critically reviewed. Unfortunately, hardly any data could be used for verification purposes due to the following reasons:

- only very few authors ([3], [18, 19]) measured experimentally the local spray angle
- most data refer to the transition regime, while the proposed model is valid for the full flashing regime (where mechanical breakup plays no role)
- the axial location where the local spray angle is measured is either not specified or confined to the downstream region (e.g. $x/D \approx 60$), where the entrainment effect becomes predominant over flashing

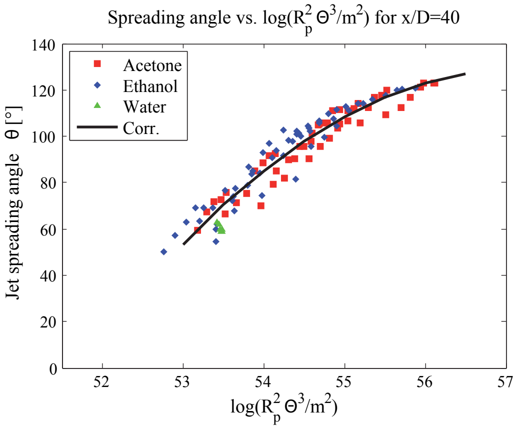

Figure 21. Comparison between the spreading angle's correlation for $x/D = 40$ and Park et al. [3] water data

Park and Lee [3] were the only authors to provide spray angle data at well-defined experimental conditions. They investigated a flashing water jet at atmospheric pressures. The pressure ratio R_p varied between $2 < R_p < 3$ (alias $20 < \Delta T < 33$ K), which corresponds to disintegration experiments in the fully flashing regime (see Fig. 10 for more details). The local spray angle was measured at the axial location $x/D = 36$. In Fig. 21, the Park and Lee data have been reduced with our modelling approach and compared to the empirical correlation obtained for the axial position $x/D = 40$.

As can be seen immediately, the Park and Lee data (in total six data points) match very well the proposed spray angle function. Although no conclusive evaluation could be drawn from this analysis, the result indicates that the proposed model might work for water jets as well.

Conclusion

The disintegration behaviour of highly superheated jet has been investigated by means of high-speed shadowgraphy. The experiments have been carried out at low pressure and near vacuum conditions, employing ethanol, acetone and iso-octane as the test fluids. The primary objective of this study is to develop a comprehensive model for the flash atomisation process. The model should provide a realistic representation of the spray contour and structure, thus enabling a reasonable initialisation of the flow field for spray simulations. As a first step, the criterion for the onset of flashing, proposed by Cleary et al. [7] for water/ethanol jets at ambient pressure, has been verified and extended to other fluids, flashing at very low back pressures. The experimental dataset is consistent with the proposed empirical correlation. The latter represents, therefore, a valid tool for predicting the inception of nucleate boiling in (highly) superheated jets.

As a second step, a generalised model for describing the jet lateral spreading has been developed, valid for an externally flashing jet. The model's underlying assumption is that bubble nucleation is the predominant mechanism controlling the shattering and lateral spreading of the jet in the near-nozzle region. By expressing the local spray angle as a function of the driving forces for nucleation (i.e. the pressure ratio R_p and non-dimensional surface tension Θ), correlations can be derived to predict the spray contour at different axial locations. These correlations are valid for different fluids and over a wide range of superheating, back pressures and injection temperatures, which confirms the generality of the correlations.

The reliability of this extended model has been tested thoroughly. These verifications showed the model can be successfully employed to reconstruct the experimental spray contour and its predictions can be generalised to fluids not included in this study with good confidence.

Acknowledgments

This work is performed within the framework of the ESA Networking and Partnering Initiative (NPI) on "Modelling Superheated (flash) atomisation and vaporisation" (ESTEC/ Contract No. 20988/08/NL/PA). The financial support of the Carl-Zeiss foundation is also gratefully acknowledged.

Nomenclature

a_0	molecular surface area	$[m^2]$
c_p	specific heat	$[J/(Kkg]$
D	nozzle diameter	$[m]$
h_{fg}	latent heat of evaporation	$[J/kg]$
J	nucleation rate	$[1/(m^3 s)]$
Ja	Jacob number $Ja = \frac{c_{pl}\Delta T}{h_{fg}} \frac{\rho_l}{\rho_v}$	$[-]$
k_b	Boltzman constant	$[J/K]$
L	nozzle length	$[m]$
m	atomic mass	$[kg]$
p	pressure	$[bar]$
R_p	pressure ratio	$[-]$
T	temperature	$[K]$
u	speed at the nozzle exit	$[m/s]$
v	molecular volume	$[m^3]$
We	Weber number $We = \frac{\rho u_0^2 D}{\sigma}$	$[-]$
x	axial position	$[m]$

Greek symbols

ΔG_n	Gibbs free energy	$[J]$
ΔT	degree of superheat	$[K]$
ΔT^*	dimensionless superheat	$[-]$
Δy	error in spray contour	$[m]$
λ	coefficient of determination	$[-]$
Ψ	correlation for the density ratio	$[-]$
ϕ	diameter	$[mm]$
ρ	density	$[kg/m^3]$
σ	surface tension	$[N/m]$
θ	spreading angle	$[-]$
Θ	dimensionless surface tension	$[-]$

Subscripts

∞	chamber conditions
inj	injection conditions
l	liquid
r	random error
s	systematic error
sat	saturation conditions
v	vapour

References

[1] R. Brown and J. L. York. *AIChE Journal*, 8:149, 1962.

[2] R. D. Oza. *Journal of Fluids Engineering*, 106:105–109, 1984.

[3] B. S. Park and S. Y. Lee. *Atomization and Sprays*, 4:159–179, 1994.

[4] H. W. M. Witlox and P. J. Bowen. Flashing liquid jets and two-phase dispersion, 2002.

[5] H. Witlox, M. Harper, P. Bowen, and V. Cleary. *American society of safety engineers - seventh professional development conference and exhibition*, pp. 236–243, Rouen, France, July 2005.

[6] Y. Kitamura, H. Morimitsu, and T. Takahashi. *Industrial and Engineering Chemistry Fundamentals*, 25:206–211, 1986.

[7] V. Cleary, P. Bowen, and H. Witlox. *Journal of Hazardous Materials*, 142:786–796, 2007.

[8] T. Kurschat, H. Chaves, and G. E. A. Meier. *Journal of Fluid Mechanics*, 236:43–59, 1992.

[9] J. R. Simoes-Moreira, M. M. Vieira, and E. Angelo. *Journal of Thermodynamics and Heat Transfer*, 16:415–424, 2002.

[10] M. M. Vieira and J. R. Simoes-Moreira. *Journal of Fluid Mechanics*, 572:121–144, 2007.

[11] H. Witlox, M. Harper, P. Bowen, and V. Cleary. *Journal of Hazardous Materials*, 142:797–809, 2007.

[12] D. Yildiz, P. Rambaud, and J. van Beeck. *5th International conference on multiphase flow*, 2004.

[13] D. Yildiz, P. Rambaud, J. van Beeck, and J. Buchlin. *ICLASS 2006*, 2006.

[14] R. Lecourt, P. Barricau, and J.Steelant. *Atomization and Sprays*, 19:106, 2009.

[15] M. Blander and J. L. Katz. *AIChE Journal*, 21:833, 1975.

[16] S. L. Girshick and C. Chiu. *J. Chem. Phys.*, 93:1273, 1990.

[17] I. Stotz, G. Lamanna, B. Weigand, and J. Steelant. *Proceedings of the 15th AIAA International Space Planes and Hypersonic Systems and Technologies Conference*, 2008.

[18] N. Nagai, K. Sato, and Ch. W. Lee. *ICLASS 85*, 1985.

[19] A. S. P. Solomon, S. D. Rupprecht, L. D-Chen, and G. M. Faeth. *Atomization and Spray Technology*, 1:53–76, 1985.